# Cross-section nano-Auger/SEM analysis to reveal bulk chemical/morphological properties of composites for energy storage

Lénaïc Madec, Jean-Bernard Ledeuil, Julien Morey, Hervé Martinez

# Cross-section nano-Auger/SEM analysis to reveal bulk chemical/morphological properties of composites for energy storage

Lénaïc Madec,[a,b,*] Jean-Bernard Ledeuil,[a] Julien Morey,[a] Hervé Martinez[a,b,c]

[a] Universite de Pau et des Pays de l'Adour, E2S UPPA, CNRS, IPREM, Pau, France
[b] Réseau sur le Stockage Electrochimique de l'Energie, CNRS FR3459, Amiens, France
[c] Centrale Casablanca, Centre de Recherche Systèmes Complexes et Interactions ; Ville Verte Bouskoura (Maroc)

* Corresponding Author: lenaic.madec@univ-pau.fr

## Abstract

Composite materials for energy storage such as powders, electrodes or battery stack often require probing their bulk chemical/morphological properties, which remains challenging so far with conventional analytical methods. In this work, $Ar^+$ milling cross-section is proposed to reveal the intrinsically buried bulk information of three different composites without physical/chemical change. Then, nano-Auger/scanning electron microscopy (SEM) analysis is proposed to investigate their bulk properties at both micro- and nano-scales. For MnCo-based powders with micrometric particles, it allowed revealing the bulk porosity and the bulk nano- or micro- Mn/Co distribution. For micrometer thick TiSnSb-based electrodes, it allowed proving the conversion reaction over long term cycling (*i.e.* the participation of the electrochemically inactive Ti) while revealing the TiSnSb particles morphological evolution (shell to core spreading/pulverization into porous structure) and SEI formation inside the porous TiSnSb. For PEO-based solid battery stacks, the cross-section allowed revealing well-defined interfaces so that reliable interfaces analysis can thus be perform. Advantage/limitation of this cross-section nano-Auger/SEM approach are also discussed. Overall, this work opens the door for future development of $Ar^+$ milling cross-section and Auger analysis as powerful tools to reveal/study buried chemical/morphological properties at micro- and nano-scales even beyond the energy storage field.

## Introduction

Composite materials and electrodes for energy storage often require probing their bulk chemical/morphological properties. However, conventional analytical methods are often limited to do so as the targeted information is intrinsically buried in the bulk of composites.

For instance, pseudocapacitive composites that have attracted interest to develop high energy supercapacitors,[1]·[2] especially for binary $MnO_2$-based composites that try to combine the high capacity of $MnO_2$ [3] to the high electronic conductivity of the second components (carbons, metals, metal oxides/hydroxides or polymers).[4]·[5] However, some questions still remain difficult to answer, especially in the case of nano-composites with a micrometric particles size: (i) What is the bulk morphological organization, *i.e.* the distribution scale of the constituents within the composites? (ii) What is the bulk structure, *i.e.* the particles size and porosity within the composites? To answer these questions, X-ray diffraction (XRD) is often used to access the size of the coherent domain but it remain limited as it cannot give access to the phase organisation within the composites. Scanning electron microscopy (SEM) and transmission electron microscopy (TEM) coupled to energy dispersive X-ray spectroscopy (EDS) remains also limited as SEM-EDS probes the micro-scale while TEM-EDS probes individual and dispersed nano-structures unlikely representative of a micrometric sample.

Another example is conversion-based electrodes that have attracted interest to develop high-energy Li-ion batteries,[6] especially for binary or ternary conversion materials that use an electrochemically inactive element to buffer the volume expansion issue (>200%).[6]·[7] However, some questions still remain difficult to answer, especially in the case of long term cycling of practical (µm thick) electrode: (i) what is the morphological evolution of the conversion material particles, *i.e.* how does the particles pulverization occur? (ii) Does the conversion reaction still occur? In addition, does the inactive element (if binary/ternary materials are used) still participate? (iii) Does the continuous solid electrolyte interphase (SEI) formation/breaking take place where the particles break up? In addition, can it be observed? To answer these questions, XRD[8]·[9] and X-ray absorption spectroscopy (XAS)[10] can be used to study/confirm the conversion reaction mechanism but they remain often limited to the first lithiation/delithiation cycle due to the fast amorphisation of binary/ternary conversion materials. *Ex situ*[11]·[12]·[13]·[14] and *in situ*[15]·[16] TEM techniques have also been widely used to study the mechanism, volume change and SEI formation of conversion materials at the nanoscale but these techniques focus on individual nano-particles, which is not representative of the reactivity occurring in three-dimensional electrodes. *In operando* X-ray tomographic microscopy (SRXTM) was also proposed to simultaneously visualize in three-dimension chemical and morphological evolution of individual particles at the electrode scale[17] but it remains limited in term of chemical information (impossibility to analyze SEI components for instance) and it often requires a synchrotron radiation.

Finally, solid-state batteries appear very attractive to improve further the energy density with longer lifetime and improved safety at an affordable cost.[18,19] However, the main current challenge to these batteries performance still remains to be overcome: How to reveal and analyze the numerous electrode materials/solid electrolyte interfaces and their electro-chemo-mechanical stability with high reliability as they are buried in battery stacks? In that direction, state-of-the-art cross-section preparation techniques such as focused ion beam (FIB) or broad ion beam (BIB, *i.e.* $Ar^+$ ion milling using a cross-polisher) have attracted interest to first reveal buried interfaces prior to their analysis by various analytical techniques.[20,21] However, these cross-section approaches remain limited so far in the case of polymer-based solid-state batteries due to the high sensitivity/degradation of polymers under ion beams exposition without specific precaution.

To tackle these issues, this work is based on the following approach (**Figure 1**): (i) specific cross-section preparations using $Ar^+$ ion milling to access the bulk of composites via the formation of flat surfaces without chemical change coupled to (ii) nano-Auger/SEM analysis to investigate the composites bulk chemical/morphological properties at micro- and nano-scales. The advantage and limitation of this cross-section nano-Auger/SEM approach is discussed regarding different composites for energy storage, namely MnCo-based powders, TiSnSb-based electrodes and a poly(ethylene oxide)-based solid-state battery stack. Overall, this work highlights the interest of $Ar^+$ milling cross-sections preparation and opens the door for future development of Auger analysis as a powerful tool to study chemical/morphological properties at both micro- and nano-scales in the field of energy storage and beyond.

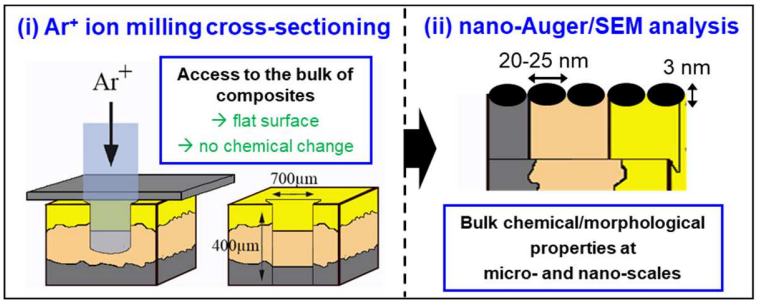


**Figure 1**. Schematic representation of the $Ar^+$ ion milling cross-sectioning and nano-Auger/SEM analysis approach followed to access and investigate the bulk chemical/morphological properties of composites at both micro- and nano-scales.

## Materials and methods

### *Composites preparation*

MnCo composite powders with a 1:1 Mn:Co ratio were prepared by exfoliation/restacking of starting H-$MnO_2$ and $\beta$3-CoOOH[22] following previously described procedures.[23]

TiSnSb synthesis, electrodes preparation (70:9:9:12 weight ratio of TiSnSb:carbon black:VGCF:CMC with 3 ±0.3 $mg_{TiSnSb}/cm^{-2}$) and cycling procedure are fully described elsewhere.[24] For clarity, cycling was performed at 25°C using 1M $LiPF_6$ EC:PC:3DMC + 5% FEC + 1% VC as electrolyte. Cells were stopped after the first lithiation at 0.02 V or after 400 cycles at 1.5 V. Before cross-section preparation, TiSnSb electrodes were washed twice by immersion in DMC (anhydrous, ≥99% purity, Aldrich, 1 ml) in a clean and dry glass vial for 10 s.

PEO-based solid-battery stack was prepared as followed: PEO (900000 g/mol, Aldrich) was first dried at 120°C under vacuum for 24h then PEO was dissolved in anhydrous acetonitrile (ACN, 99.8%, Aldrich) by magnetic stirring at 50°C for 48h under argon. Lithium bis(trifluoromethanesulfonyl)imide (LiTFSI, 99.95%, Aldrich) was then added with a 25 :1 $O_{PEO}$:$Li_{LiTFSI}$ ratio and kept under stirring for 24h. The obtained gel was then infused into NMC532 electrodes (S4R Montpellier, ~11.5 $mg/cm^2$, pressed at 2 tons, ~50 µm thick, ~30% porosity) and graphite electrodes (S4R Montpellier, ~6.1 $mg/cm^2$, pressed at 2 tons, ~50 µm thick, ~30% porosity) deposited in CR2032 coin cell cases. The ACN was then slowly evaporated using a specific heating procedure (30 min at 30°C, 50°C, 60°C and 1h at 70°C), which allowed filling the entire electrodes porosity by the PEO-LiTFSI electrolyte. Note that an excess of gel was used so that the PEO-LiTFSI electrolyte not only filled the electrode porosity but also formed a thin film covering the electrodes. Finally, a full solid-state polymer-based battery stack was assembled by putting into contact the two PEO-LiTFSI based electrodes at 70°C for 24h.

***Cross-section preparation of the composites using $Ar^+$ ion milling***

**Figure 2 top** shows the schematic representation of the specific sample preparation followed prior to the cross-sectioning by $Ar^+$ ion milling as function of the composites. For all samples, preparation was performed in a nitrogen-filled glove-box. For MnCo, the powders were hand-mixed in a conducting silver-charged epoxy resin (to limit possible charging effect during Auger/SEM analysis) then deposited on a silicon wafer. Then the whole was fixed to a JEOL sample holder with the same epoxy resin. For TiSnSb, electrodes were sandwiched between two silicon wafers using a conducting silver-charged epoxy resin. Then the whole was fixed to a JEOL sample holder with the same epoxy resin. Finally, the MnCo and TiSnSb assemblies were then cross-sectioned at normal angle from the silicon wafer using a mask directly in contact with the silicon wafer. For PEO-based solid-battery, the stack was first thinned using a vertical slicer then deposited on a copper foil (GoodFellow, 99.97%, 100 µm thick) with a conductive carbon glue (Pelco). The whole was then fixed to a Technoorg LINDA sample holder with the same conductive carbon glue. Finally, the PEO-based assembly was then cross-sectioned at normal angle from the top of the assembly using a mask positioned at about 20 µm.

For MnCo composite powders and TiSnSb composite electrodes, cross-sections were obtained using a JEOL cross-Polisher (JEOL Ltd, Tokyo, Japan) working at 1.0 $x10^{-4}$ Pa with an $Ar^+$ beam of 6 keV, ~120 µA (emission current) for 4h or 8h, respectively. For the PEO-based solid-battery stack, cross-section was obtained using a SEMPrep2 cross-Polisher (Technoorg LINDA) working

at 1.4 x$10^{-4}$ Pa with an $Ar^+$ beam of 8 keV, 3.5 mA (*i.e.* 250 µA emission current) for 6h under liquid nitrogen cooling (133°K) to supress possible polymer degradation. Note that the use of the copper foil and the conductive carbon glue was also used to improve further the cooling of the assembly.

Overall, planar surfaces were obtained for all composites (**Figure 2 bottom**). However, $Ar^+$ milling is known to often lead to material re-deposition due to the sputtering process thus inducing possible curtaining effect, especially for samples with pores. Importantly, note that no chemical change is expected as $Ar^+$ milling is known to limit sample damage to amorphisation with the same chemical composition together with $Ar^+$ implantation[25]·[26]·[27] that was never observed in our case (no Ar LMM Auger lines at 211 and 195 eV in KE).

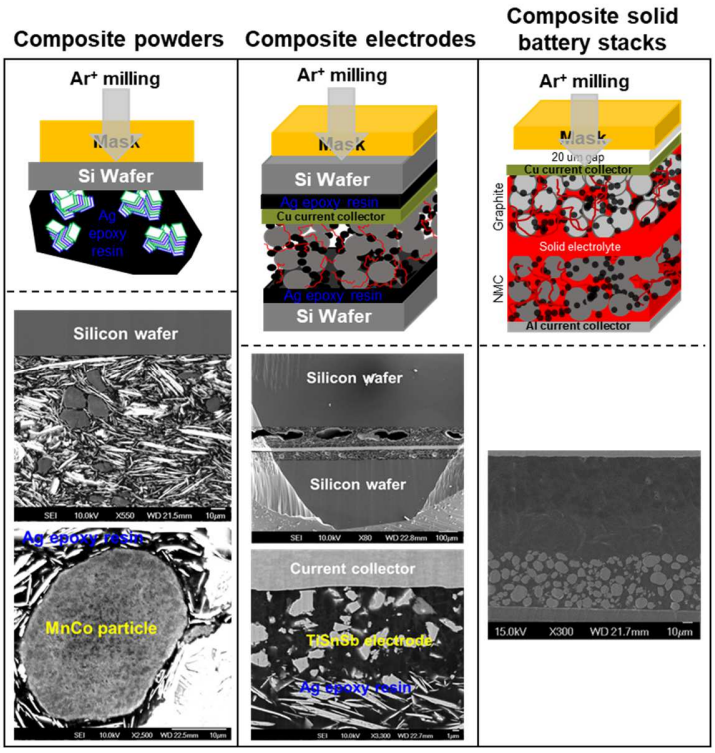


**Figure 2**. (top) Schematic representation of the specific sample preparation followed prior to the $Ar^+$ milling cross-sectioning as function of the composites and (bottom) resulting typical low magnification SEM images showing the planar surface obtained by the $Ar^+$ milling cross-sectioning. The white/grey flakes observed in SEM images correspond to the silver epoxy resin.

***Scanning electron microscopy (SEM), Auger electron spectroscopy (AES) and scanning Auger microscopy (SAM)***

Importantly, the probe size for AES (*i.e.* to record an Auger spectrum) is about 20 nm leading to a spatial resolution for SAM (*i.e.* to record an Auger image) of about 25 nm while the probing depth is about 2-3 nm in the analysis conditions used. Thus, the simultaneous presence of different Auger transitions from different elements (Ti + Sn + Sb or Mn + Co for instance) in a spectrum means that these elements coexist, *i.e.* are located together in a 25 nm wide area with a 3 nm depth.

SEM, AES and SAM were performed using a JEOL JAMP 9500 F Auger spectrometer (JEOL Ltd, Tokyo, Japan) equipped with a Schottky Field Emission gun and a hemi-spherical analyser coupled with a high dynamic multichannel detector. The operating pressure was $<2 \times 10^{-7}$ Pa and analysis were performed at 30-40° tilt to prevent charging effect except for thickness measurement that were done at 0° tilt. For Auger analysis, the electron beam was fixed at 10 keV/5 nA for MnCo and TiSnSb or at 15 keV/5 nA for the PEO-based stack. AES survey spectra were recorded with 1 eV step size using a focused probe and a CRR mode (constant relative resolution) with a constant relative energy resolution dE/E= 0.5% (high sensitivity). Auger spectra are presented using the EN(E) mode expressed as the output signal of the electron detector using "true" pulse counting versus kinetic energy. SAM (elemental 2D distribution images) were recorded using a CAE mode (constant analyzer energy) corresponding to a fixed energy resolution. SAM images are represented using "peak minus background" (P-B) Auger intensity for a transition (dE/E=0.5%). An "auto probe tracking" correction was also applied to control and compensate any potential drift during acquisition.

## Results and discussion

***MnCo-based powders*** – It is reminded that these composites (noted RMC1a, RMC1b and RMC2) were prepared from the exfoliation/restacking of H-$MnO_2$ and $\beta$3-CoOOH following different procedures that are summarized on **Figure 3** for better clarity. Note first that previous XRD analysis showed that the thickness of Mn-based domains decrease while it did not change for Co-based domains (except for RMC1a).[23] However, no conclusion was obtained from XRD about the phase organisation within the composites. Thus, SEM/nano-Auger analysis was performed on these composites cross-section to investigate the exact bulk structure (porosity) and bulk morphological organization (Mn / Co distribution scale), **Figure 3**. SEM images showed a highly porous bulk structure for RMC1a and RMC2 (**Figure 3a** and **3c**, respectively) in agreement with their high specific BET surface area (about 95 $m^2/g$ [23]). At the opposite, RMC1b (**Figure 3b**) showed a dense bulk structure, *i.e.* a closed porosity that explains its low specific BET surface area (2 $m^2/g$) due to the slow acidification step used to flocculate the Mn- and Co- nano-sheets. Regarding the nano-Auger analysis, Auger survey spectra showed O KLL, Mn LMM and Co LMM transitions at about 500 and 480 eV, at about 630, 580 and 530 eV and at about 775, 710 and 645 eV, respectively. SAM overlay images (*i.e.* elemental 2D distribution from Mn LMM in

blue and Co LMM in green) for RMC1a and RMC1b (**Figure 3a** and **3b**, respectively) suggest a nanoscale distribution of Mn / Co. This was further confirmed by Auger survey spectra that always showed Mn and Co LMM transitions simultaneously, *i.e.* within the 20 nm wide and 2-3 nm depth probe size. Thus, for RMC1a and RMC1b, the restacking procedure occurred at the nanoscale, *i.e.* the Mn / Co distribution scale is lower than 20 nm. At the opposite, the SAM overlay image for RMC2 (**Figure 3c**) clearly suggest a microscale distribution of Mn / Co, which is confirmed by Auger survey spectra showing either Mn or Co LMM transitions, which highlights the importance of the restacking procedure. Indeed, contrary to RMC1a and RMC1b, the acidification for RMC2 was performed before mixing the colloidal suspensions together thus favoring the flocculation before an intimate mixture could be obtained. As a result, RMC1a and RMC1b (**Figure 3a** and **3b**, respectively) are nano-composites while RMC2 (**Figure 3c**) is a micro-composite.

Overall, the cross-section SEM/nano-Auger analysis is of high interest to investigate the bulk structure (porosity) together with the bulk morphological organization (distribution scale) of nano-composites powders with micrometric particles size, which remained a challenge so far. At this point, note that higher magnification could be used to get further insight about the nanoscale distribution but this remains limited by the lack of topographic contrast for such flat samples. An alternative would be to use backscattered electrons to get a Z (atomic number) contrast between elements thus enabling higher magnification/resolution but this mode is not present in our Auger system so far.

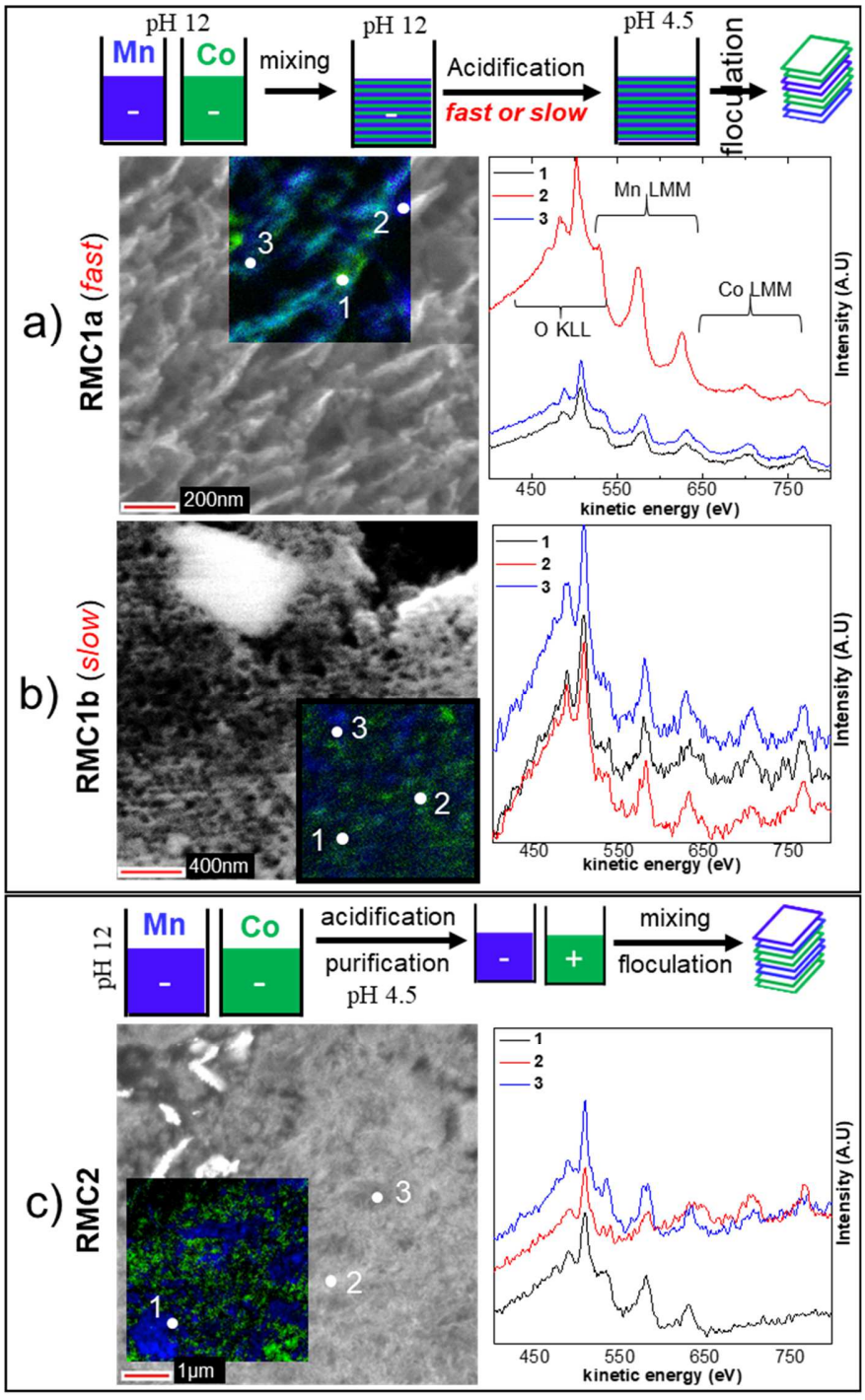


**Figure 3**. SEM images with SAM overlay (elemental 2D distribution from Mn LMM in blue and Co LMM in green) and Auger spectra taken at indicated positions for the different MnCo composite powders, namely, a) RMC1a, b) RMC1b and c) RMC2. The corresponding exfoliation/restacking procedures are also summarized for clarity.

***TiSnSb-based electrodes*** – **Figure 4a**, the SEM image of the TiSnSb electrode cross-section before cycling showed dense and shapeless TiSnSb particles of 0.5-5 µm surrounded by large and porous areas containing the carbon additives and the CMC binder as confirmed by SAM images and Auger survey spectra. After the 1st lithiation at 25°C (**Figure 4b**), TiSnSb particles remained dense with a relatively homogeneous lithiation over the entire electrode thickness as observed from the SAM images. Note that some particles at the bottom were not lithiated more likely because they are not connected to the electronic conductive carbon network of the electrode as observed by SEM (**Figure 4b**). After 400 cycles at 25°C (**Figure 4c**), the morphology of the TiSnSb particles significantly changed with the formation of non-uniform porous shell surrounding dense core as observed from both SEM and SAM images. Particles cracks located in the dense cores were also observed (SEM image, **Figure 4c**). This result thus suggests a shell to core spreading/pulverization of TiSnSb particles over long term cycling. This TiSnSb particles volume expansion phenomenon led to a filling of the electrode porosity as well as to an increase of the electrode thickness, from 12 ±2 µm for the electrode before cycling (**Figure 4a**) to 15 ±2 µm after the 1st lithiation (**Figure 4b**) and finally to 50 ±3 µm after 400 cycles (**Figure 4c**). Importantly, the Ti, Sn and Sb distribution at the nanoscale (*i.e.* within the 30 nm wide and 2-3 nm depth resolution for the SAM images) remained relatively homogeneous with only small discrepancies located on the porous shells and despite the huge volume expansion (*i.e.* huge TiSnSb particles spreading) over long term cycling. This result thus proves that the conversion reaction of TiSnSb into $Li_3Sb/Li_7Sn_2/Ti$ still occurs even after 400 cycles. It also proves that the electrochemically inactive Ti element still participate to the reaction. Finally, after 400 cycles (**Figure 4c**), fluorine and oxygen elements are detected due to the formation of F- and O-containing SEI species formed by the electrolyte degradation. Interestingly, the SAM images of C, O, F KLL and Ti LMM as well as SAM overlay images of C/O/F and C/O/Ti showed that oxygen and fluorine are located in the porous TiSnSb areas while they are absent from the carbon additive areas. This result thus points to an SEI formation inside the TiSnSb porous shell, in other words as the TiSnSb particles continuously pulverize/break up to form fresh surface over long term cycling.

Overall, the cross-section SEM/nano-Auger analysis is of high interest to investigate both the morphological evolution and reaction of conversion materials together with the observation of the SEI formation for micrometer thick electrode and over long term cycling, which remained a challenge so far. At this point, note that one advantage of this approach is the possibility to detect and map the lithium element distribution contrary to most of the analytical techniques including surface sensitive ones. Of course, this remains true only if no other elements overlap with the Li KVV transition such as for Fe.

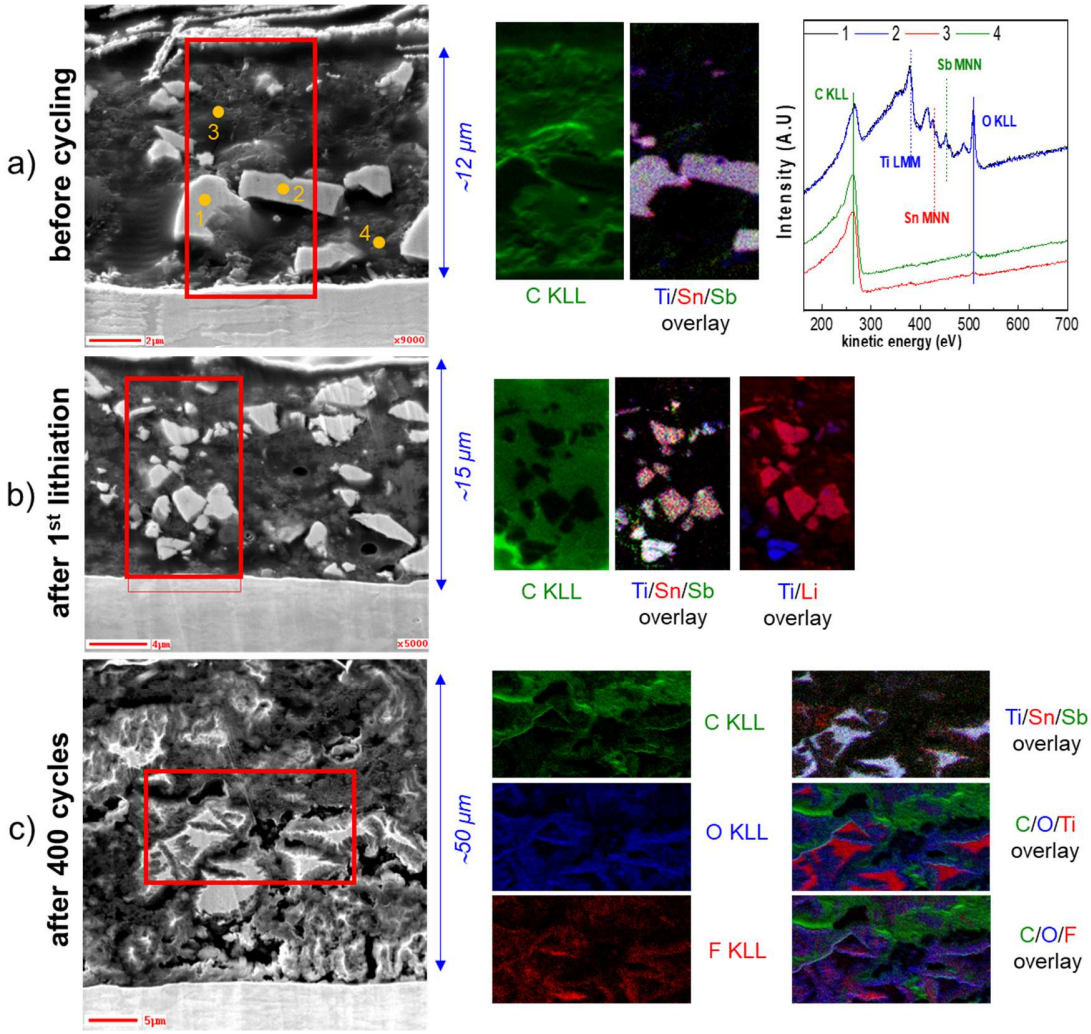


**Figure 4**. SEM images of TiSnSb electrodes cross-section a) before cycling, b) after the 1st lithiation at 25°C and c) after 400 cycles at 25°C with selected SAM (elemental 2D distribution) images from C KLL, O KLL, F KLL, Li KVV, Ti LMM, Sn MNN, Sb MNN transitions and some overlays. The area at which the SAM images were taken is indicated in the SEM images. For the TiSnSb electrodes cross-section before cycling (a), Auger spectra are also presented as taken at different position as indicated in the SEM image.

***PEO-based solid-state battery stack*** – It is reminded (as described in the experimental part) that one NMC/PEO-LiTFSI/graphite stack cross-section was typically obtained without optimized $Ar^+$ milling parameters (**Figure 5a**) while the other one was obtained with optimized $Ar^+$ milling parameters (**Figure 5b**). Without optimization (**Figure 5a**), the SEM image showed that a rough surface was obtained with polymer flowing over the entire cross-section and delamination at the NMC electrode top surface. Such phenomena were partially expected as constraints produced by the $Ar^+$ beam can easily damage polymers due to heat dissipation. Therefore, various $Ar^+$ beam

conditions were tested, *i.e.* ion beam voltage between 6-16 kV with 2 keV step, ion beam current between 2-4 mA (*i.e.* 300 µA emission current) with 0.5 step and for different times but always under liquid nitrogen cooling (133 K). Once $Ar^+$ milling parameters were optimized (8 keV, 3.5 mA, 6h at 133 K), the SEM image (**Figure 5b**) showed that a perfectly flat cross-section surface was obtained without apparent physical damage such as polymer flowing. Indeed, the morphology of the different layers and the different interfaces were well defined while the thickness of the layers was preserved. This is supported by SAM images (**Figure 5b**) of Al KLL (current collector), Co LMM (NMC), S KLL (LiTFSI) and F KLL (LiTFSI + PVDF) showing well defined areas with no spreading/flowing. Interestingly, SAM images of S and F KLL showed that the PEO-LiTFSI electrolyte filled the electrode porosity over the entire electrode thickness. This result highlights that the electrode infusion method by the PEO-LiTFSI/ACN gel followed by the gradual evaporation of ACN is very powerful even for such 50 µm thick electrodes. Finally, typical Auger spectrum (**Figure 5b**) of an NMC particle taken after $Ar^+$ cross-sectioning showed that no chemical change was observed compared to the spectrum of the corresponding pristine NMC powder, *i.e.* the line shapes matched perfectly and no new transition appeared. Note that this was further confirmed by X-ray spectroscopy analysis (not shown here).

Overall, the $Ar^+$ milling cross-section approach is of very high interest to reveal at once all interfaces buried in polymer-based solid-state batteries without physical/chemical damage and despite the high sensitivity of the polymers, which remained a challenge so far. As a matter of fact, to our knowledge, it is the first time this approach is proposed/applied in the literature. At this point, the main drawback of this approach is the possible need for $Ar^+$ milling parameters optimization as function of the battery stack system. However, in our case, it was possible to cross-section other battery stacks based on different polymer or gel electrolytes using the optimized ion beam voltage/current while changing only the time due to different stacks thicknesses.

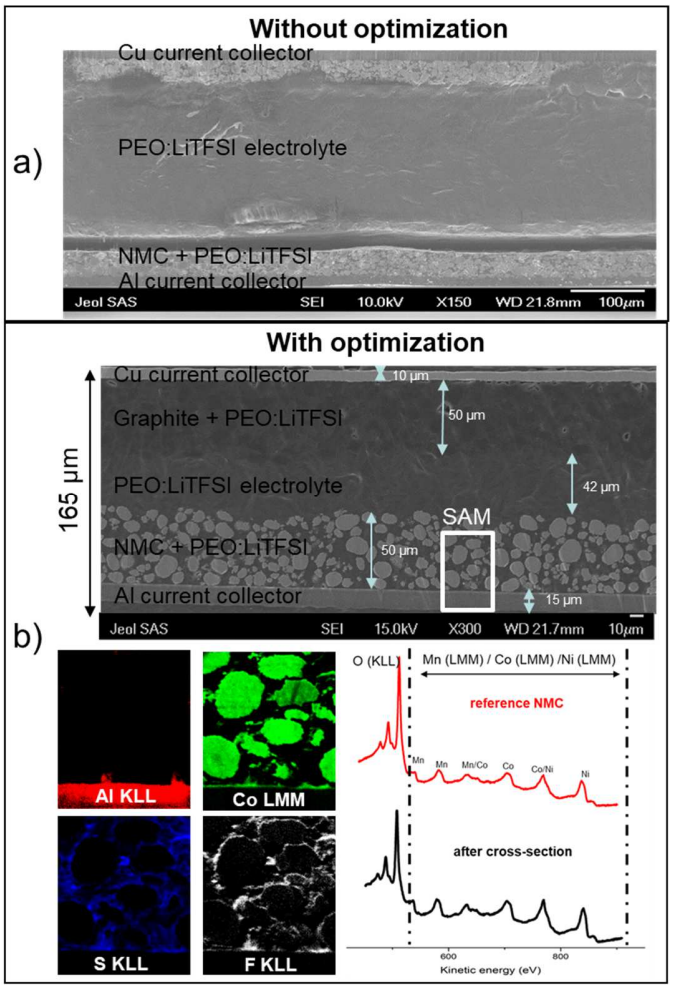


**Figure 5**. SEM images of NMC/PEO-LiTFSI/graphite stack cross-sections a) without and b) with optimized $Ar^+$ milling parameters. For the optimized cross-section (b), selected SAM (elemental 2D distribution) images taken at the indicated position from Al KLL, Co LMM, S KLL and F KLL are also presented together with a typical Auger spectrum of an NMC particle compared to a reference spectrum of the corresponding pristine NMC powder.

## Conclusions

In this work, cross-section by $Ar^+$ ion milling is proposed as a powerful method used to access the bulk of composites without physical/chemical change. The sample preparation conditions prior to the $Ar^+$ milling cross-sectioning are thus fully described as function of the composites. Moreover, nano-Auger/SEM analysis is proposed to investigate bulk chemical/morphological properties at both micro- and nano-scales for different energy storage composites, namely MnCo-based powders, TiSnSb-based electrodes and PEO-based solid-state battery stacks. For MnCo powders, it allowed revealing the bulk porosity together with the bulk nano- or micro- Mn/Co distribution

for micrometric particles. For TiSnSb electrodes, it allowed proving the conversion reaction (and thus the participation of the electrochemically inactive Ti) while revealing the TiSnSb particles morphological evolution (shell to core spreading/pulverization into porous structure) and SEI formation inside the porous TiSnSb, all for micrometer thick electrode over long term cycling. For PEO-based stacks, the cross-section preparation allowed revealing well-defined buried interfaces, which will then be used to follow the interfaces evolution over cycling. Finally, the main advantage and limitation of this cross-section nano-Auger/SEM approach are discussed for each composites. Interestingly, note that the last generation of Auger apparatus has the capacity to perform *in situ* focused ion beam (FIB) cross-sectioning, which should further increase the interest of this method with minimum sample preparation.

Overall, this work thus opens the door for future development of both $Ar^+$ milling cross-section preparation and Auger analysis as powerful tools to reveal and study buried chemical/morphological properties at both micro- and nano-scales in the field of energy storage and beyond, which remained a challenge so far.

## Acknowledgment

This research was performed in the framework of "Réseau sur le Stockage Electrochimique de l'Energie" (RS2E) and the ANR program no. ANR-10-LABX-76-01. The PEO-based solid-state battery part was carried out as part of the HUB RAISE2024 project funded by Excellence Initiative of Université de Pau et des Pays de l'Adour, I-Site E2S, a French "Investissements d'Avenir" programme.

## References

[1] L.L. Zhang, R. Zhou, X.S. Zhao, Graphene-based materials as supercapacitor electrodes, J. Mater. Chem. 20 (2010) 5983–5992. https://doi.org/10.1039/c000417k.

[2] V. Augustyn, P. Simon, B. Dunn, Pseudocapacitive oxide materials for high-rate electrochemical energy storage, Energy Environ. Sci. 7 (2014) 1597–1614. https://doi.org/10.1039/c3ee44164d.

[3] M. Toupin, T. Brousse, D. Bélanger, Charge storage mechanism of MnO2 electrode used in aqueous electrochemical capacitor, Chem. Mater. 16 (2004) 3184–3190. https://doi.org/10.1021/cm049649j.

[4] W. Wei, X. Cui, W. Chen, D.G. Ivey, Manganese oxide-based materials as electrochemical supercapacitor electrodes, Chem. Soc. Rev. 40 (2011) 1697–1721. https://doi.org/10.1039/c0cs00127a.

[5] J.G. Wang, F. Kang, B. Wei, Engineering of MnO<inf>2</inf>-based nanocomposites for high-performance supercapacitors, Prog. Mater. Sci. 74 (2015) 51–124.

https://doi.org/10.1016/j.pmatsci.2015.04.003.

[6] V. Aravindan, Y.S. Lee, S. Madhavi, Research Progress on Negative Electrodes for Practical Li-Ion Batteries: Beyond Carbonaceous Anodes, Adv. Energy Mater. 5 (2015) 1402225. https://doi.org/10.1002/aenm.201402225.

[7] A. Mukhopadhyay, B.W. Sheldon, Deformation and stress in electrode materials for Li-ion batteries, Prog. Mater. Sci. 63 (2014) 58–116. https://doi.org/10.1016/j.pmatsci.2014.02.001.

[8] M.T. Sougrati, J. Fullenwarth, A. Debenedetti, B. Fraisse, J.C. Jumas, L. Monconduit, TiSnSb a new efficient negative electrode for Li-ion batteries: mechanism investigations by operando-XRD and Mössbauer techniques, J. Mater. Chem. 21 (2011) 10069–10076. https://doi.org/10.1039/c1jm10710k.

[9] H. Ikeda, S. Narukawa, Behaviour of various cathode materials for non-aqueous lithium cells, J. Power Sources. 9 (1983) 329–334. https://doi.org/10.1016/0378-7753(83)87035-9.

[10] M. Fehse, A. Darwiche, M.T. Sougrati, E.M. Kelder, A. V. Chadwick, M. Alfredsson, L. Monconduit, L. Stievano, In-Depth Analysis of the Conversion Mechanism of TiSnSb vs Li by Operando Triple-Edge X-ray Absorption Spectroscopy: A Chemometric Approach, Chem. Mater. 29 (2017) 10446–10454. https://doi.org/10.1021/acs.chemmater.7b04088.

[11] S. Grugeon, S. Laruelle, R. Herrera-Urbina, L. Dupont, P. Poizot, J.-M. Tarascon, Particle Size Effects on the Electrochemical Performance of Copper Oxides toward Lithium, J. Electrochem. Soc. 148 (2001) A285–A292. https://doi.org/10.1149/1.1353566.

[12] J.-M. Tarascon, S. Grugeon, M. Morcrette, S. Laruelle, P. Rozier, P. Poizot, New concepts for the search of better electrode materials for rechargeable lithium batteries, Comptes Rendus Chim. 8 (2005) 9–15. https://doi.org/10.1016/j.crci.2004.12.005.

[13] D. Yonekura, E. Iwama, N. Ota, M. Muramatsu, M. Saito, Y. Orikasa, W. Naoi, K. Naoi, Progress of the conversion reaction of Mn3O4particles as a function of the depth of discharge, Phys. Chem. Chem. Phys. 16 (2014) 6027–6032. https://doi.org/10.1039/c4cp00334a.

[14] F. Wang, R. Robert, N.A. Chernova, N. Pereira, F. Omenya, F. Badway, X. Hua, M. Ruotolo, R. Zhang, L. Wu, V. Volkov, D. Su, B. Key, M. Stanley Whittingham, C.P. Grey, G.G. Amatucci, Y. Zhu, J. Graetz, Conversion reaction mechanisms in lithium ion batteries: Study of the binary metal fluoride electrodes, J. Am. Chem. Soc. 133 (2011) 18828–18836. https://doi.org/10.1021/ja206268a.

[15] N. Liu, Z. Lu, J. Zhao, M.T. Mcdowell, H.W. Lee, W. Zhao, Y. Cui, A pomegranate-inspired nanoscale design for large-volume-change lithium battery anodes, Nat. Nanotechnol. 9 (2014) 187–192. https://doi.org/10.1038/nnano.2014.6.

[16] Q. Su, J. Xie, J. Zhang, Y. Zhong, G. Du, B. Xu, In Situ Transmission Electron Microscopy Observation of Electrochemical Behavior of CoS 2 in Lithium-Ion Battery, ACS Appl. Mater. Interfaces. 6 (2014) 3016–3022. https://doi.org/10.1021/am4056084.

[17] M. Ebner, F. Marone, M. Stampanoni, V. Wood, Visualization and Quantification of Electrochemical and Mechanical Degradation in Li Ion Batteries, Science (80-. ). 342 (2013) 716–720. https://doi.org/10.1126/science.1241882.

[18] A. Manthiram, X. Yu, S. Wang, Lithium battery chemistries enabled by solid-state electrolytes, Nat. Rev. Mater. 2 (2017). https://doi.org/10.1038/natrevmats.2016.103.

[19] Q. Zhang, K. Liu, F. Ding, X. Liu, Recent advances in solid polymer electrolytes for lithium batteries, Nano Res. 10 (2017) 4139–4174. https://doi.org/10.1007/s12274-017-1763-4.

[20] T.T. Zuo, R. Rueß, R. Pan, F. Walther, M. Rohnke, S. Hori, R. Kanno, D. Schröder, J. Janek, A mechanistic investigation of the Li10GeP2S12|LiNi1-x-yCoxMnyO2 interface stability in all-solid-state lithium batteries, Nat. Commun. 12 (2021). https://doi.org/10.1038/s41467-021-26895-4.

[21] I. López, J. Morey, J.B. Ledeuil, L. Madec, H. Martinez, A critical discussion on the analysis of buried interfaces in Li solid-state batteries.: Ex situ and in situ / operando studies, J. Mater. Chem. A. 9 (2021) 25341–25368. https://doi.org/10.1039/d1ta04532f.

[22] C. Tang, D. Giaume, L. Guerlou-Demourgues, G. Lefèvre, P. Barboux, Prediction of Isoelectric Point of Manganese and Cobalt Lamellar Oxides: Application to Controlled Synthesis of Mixed Oxides, Langmuir. 34 (2018) 6670–6677. https://doi.org/10.1021/acs.langmuir.8b00190.

[23] C. Tang, D. Giaume, F. Weill, N. Penin, M.A. Dourges, H. Saadaoui, L. Guerlou-Demourgues, Synergy of Mn and Co in Slab-Based Nanocomposites for Hybrid Supercapacitors: Impact of Restacking Process on Electrochemical Properties, ACS Appl. Energy Mater. (2019). https://doi.org/10.1021/acsaem.9b01263.

[24] L. Madec, G. Gachot, G. Coquil, H. Martinez, L. Monconduit, Toward efficient Li-ion cells at high temperatures: Example of TiSnSb material, J. Power Sources. 391 (2018) 51–58. https://doi.org/10.1016/j.jpowsour.2018.04.068.

[25] T. Schuhrke, M. Mändl, J. Zweck, H. Hoffmann, Investigation of surface amorphization of silicon wafers during ion-milling, Ultramicroscopy. 41 (1992) 429–433. https://doi.org/10.1016/0304-3991(92)90223-7.

[26] J.P. McCaffrey, M.W. Phaneuf, L.D. Madsen, Surface damage formation during ion-beam thinning of samples for transmission electron microscopy, Ultramicroscopy. 87 (2001) 97–104. https://doi.org/10.1016/S0304-3991(00)00096-6.

[27] M. Mitome, Ultrathin specimen preparation by a low-energy Ar-ion milling method, J. Electron Microsc. (Tokyo). 62 (2013) 321–326. https://doi.org/10.1093/jmicro/dfs073.